Journal of Materials Chemistry A

Vertically Aligned MoS_2 on Ti_3C_2 (MXene) as an Improved HER Catalyst

Journal:	*Journal of Materials Chemistry A*
Manuscript ID	TA-COM-05-2018-005033.R2
Article Type:	Communication
Date Submitted by the Author:	03-Aug-2018

Complete List of Authors:	Attanayake, Nuwan; Temple University, Department of Chemistry; Center for Computational Design of Functional Layered Materials (CCDM), Temple University Abeyweera, Sasitha; Temple University, Department of Chemistry Thenuwara, Akila; Temple University, Chemistry; Center for Computational Design of Functional Layered Materials (CCDM), Temple University Anasori, Babak; Drexel University, Materials Science and Engineering Gogotsi, Yury; Drexel University, Department of Materials Science & Engineering, and A. J. Drexel Nanomaterials Institute Sun, Yugang; Temple University, Department of Chemistry Strongin, Daniel; Temple University, Chemistry; Center for Computational Design of Functional Layered Materials (CCDM), Temple University

Journal Name COMMUNICATION

Vertically Aligned MoS_2 on Ti_3C_2 (MXene) as an Improved HER Catalyst

Nuwan H. Attanayake,[a,b] Sasitha C. Abeyweera,[a] Akila C. Thenuwara,[a,b] Babak Anasori,[c] Yury Gogotsi,[c] Yugang Sun,[a] Daniel R. Strongin.[*,a,b]

[a.]Department of Chemistry, Temple University, 1901 N. 13th Street, Philadelphia, PA 19122 (USA)

[b.]Center for Computational Design of Functional Layered Materials (CCDM)

[c.]Department of Materials Science and Engineering, and A.J. Drexel Nanomaterials Institute, Drexel University, Philadelphia, PA 19104 (USA)

*Email - dstrongi@temple.edu

Abstract

We have demonstrated the microwave-assisted growth of vertically aligned interlayer expanded MoS_2 on conductive two-dimensional Ti_3C_2 MXene nanosheets ($MoS_2 \perp Ti_3C_2$) and investigated the produced material as an electrocatalyst for the hydrogen evolution reaction (HER). $MoS_2 \perp Ti_3C_2$ offers a unique inorganic hybrid structure that allows an increased exposure of catalytically active edge sites of MoS_2, compared to pure MoS_2 with a platelet-like morphology. The vertically aligned few-layer MoS_2 sheets have an expanded interlayer spacing of 9.4 Å. The $MoS_2 \perp Ti_3C_2$ catalyst exhibited a low onset potential (-95 mV vs RHE) for the HER and a low Tafel slope (~40 mV dec^{-1}). The catalyst maintained a steady catalytic activity for the HER for over 20 hours.

Text

The storage of electrical energy generated from solar to a large enough extent is still limited by the relatively low energy storage capacities of current devices, such as batteries. A feasible way to larger-scale storage is to use chemical bonds to store potential energy. Hydrogen is one of the most important molecules in the context of energy storage.[1-4] Using photovoltaics to convert solar energy to electric energy and using electrolyzers to reduce protons to hydrogen gas through water splitting is an attractive solution.[5] Stable and efficient electrolyzers are an important part of the process and the search for Earth abundant materials that can catalyze the reduction of protons with the lowest possible energy is an active area of research.[6]

Theoretical investigations of the hydrogen evolution reaction (HER) have suggested that materials which display low binding free energies for atomic hydrogen ($\Delta G_H \sim 0$) are the most suitable candidates.[7-8] In particular, it has been shown that the edge sites of 2-dimensional (2D) MoS_2 sheets are associated with ΔG_H values close to zero.[6, 9-10] Relatively weak van der Waals forces bind the 2D MoS_2 sheets into a layered structure with an interlayer spacing of ~6.2 Å.[10-12] Two polymorphic forms of MoS_2 have been studied extensively for HER: the semiconducting 2H (trigonal prismatic co-ordination) and the metallic 1T (octahedral co-ordination) phase. 2H-MoS_2 is the more stable phase and prior research has shown that the basal plane of this phase is largely inactive towards the electrochemical HER.[6, 9, 11, 13-14] The 1T-MoS_2 phase has been shown to have a higher electrical conductivity along both the basal plane and at its edges making it a better HER electrocatalyst than 2H-MoS_2.[13, 15] The long term instability of 1T-MoS_2 for the HER has prevented 1T-MoS_2 from being an optimal catalyst. Thus, considerable effort has been expended to create 2H-MoS_2 nanostructures that optimize the exposure of edges and which exhibit an improved conductivity.[16-20]

Recent research[17] has shown that expansion of the interlayer spacing of MoS_2 improves HER catalysis.[21] The growth of vertically aligned interlayer expanded MoS_2 (IE-MoS_2) on conductive substrates and scaffolds have been shown to lead to materials with efficient charge transfer from electrode to catalyst and more exposed edge sites.[22] Many carbon based materials have been extensively studied as the conductive support for MoS_2 and other HER catalysts .[23-25] Carbon nanotubes (CNTs),[26-27] carbon cloth,[28-29] graphene oxide/reduced graphene oxide (GO/rGO),[18, 30-32] amorphous carbon supports,[33] and glassy carbon[20, 34] have all been studied as support materials. In this study, we present

a novel method to grow vertically aligned MoS_2 directly on a 2D layered inorganic material, titanium carbide (Ti_3C_2) to further improve HER catalysis for IE-MoS_2. Ti_3C_2 belongs to the family of 2D transition metal carbides and nitrides, called MXenes.[35-40] MXenes have the general formula $M_{n+1}X_nT_x$, where, M is an early transition metal (Ti, V, Nb, Mo, etc.), X is carbon or nitrogen, and n= 1-3. T_x is the surface termination group (typically -O, -OH or –F) left after the selective extraction of certain atomic layers in a top-down etching process of their precursors. More than twenty different MXenes have been synthesized and studied to date, such as Ti_2CT_x, Mo_2CT_x, $Ti_3C_2T_x$, V_2CT_x, $Mo_2TiC_2T_x$.[38] We drop the T_x notation referring to the surface termination when referring to the samples in the current study. MXenes are mostly metallic (conductivity is up to 9880 S/cm for Ti_3C_2),[40] because of their metal carbide core layers, and hydrophilic due to their surface terminations.[35-37] Conductivity of Ti_3C_2 MXene, is higher than that of CNTs,

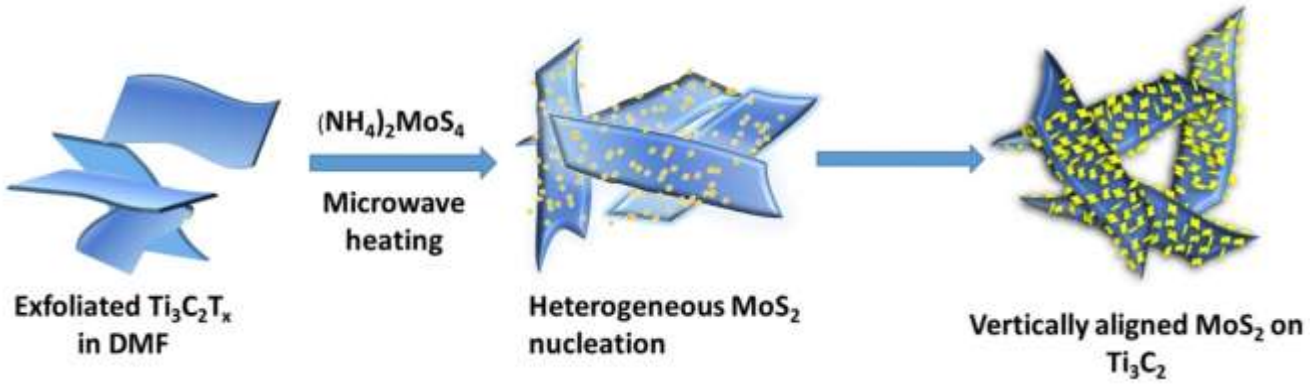

Scheme 1: Schematic of the synthesis process for the growth of vertically aligned IE-MoS_2/Ti_3C_2. In the first step, Ti_3C_2 flakes were homogeneously distributed in DMF by sonication and then $(NH_4)_2MoS_4$ was added to the Ti_3C_2 loaded DMF solution. Exposure of the $(NH_4)_2MoS_4$ and Ti_3C_2 containing solution to microwave radiation led to the nucleation and then vertically oriented growth of MoS_2 on the conductive Ti_3C_2 support.

graphene or GO materials, which makes it an excellent candidate to support MoS_2 catalyst for the HER.[40]

Our hypothesis that motivates the present study is that vertically aligned IE-MoS_2 grown on Ti_3C_2 will serve as an excellent HER catalyst. The hypothesis rests largely on the realization that Ti_3C_2 exhibits a metal-like conductivity, likely making it a better substrate than GO for the growth of vertically aligned MoS_2.[41-42] The conductivity between the substrate and catalyst is a crucial factor in determining the charge transfer kinetics of the catalyst. Exfoliated Ti_3C_2 MXenes provide a large surface area and moreover show better conductivity than reduced graphene/GO and most other 2D materials hence, Ti_3C_2 would make a superior substrate for the growth of MoS_2 .[24, 38, 40, 43-44] Furthermore, we hold out the possibility that a higher density of vertically aligned MoS_2 layers can be grown on Ti_3C_2 than can be grown on the more studied graphene support.[18, 30-32, 45] The hydrophilicity of the MXene support can aid the binding of ionic precursors (MoS_4^{2-}) on their surfaces and dispersion in polar solvents unlike hydrophobic graphene supports.

To grow vertically aligned MoS_2 on Ti_3C_2, we used a microwave assisted colloidal synthetic method. Ammonium tetrathio molybdate ($(NH_4)_2MoS_4$) in N,N-dimethyl formamide (DMF) was used as the precursor solution for IE-MoS_2.[17] Microwaves interacting with charges on the MXene sheets generates the heat that help nucleate MoS_2 sheets on a support as depicted in Scheme 1.[32, 46-48] Ti_3C_2 was expected to be an ideal surface for this process, since it provides metallic conductivity, a large surface area, and a charged surface for nucleation and growth of MoS_2. We support this contention by noting that prior studies have shown that Ti_3C_2 exhibits a very high absorption of electromagnetic waves (e.g., in the microwave region), even at very small thicknesses.[49-

The synthesis of IE-MoS_2 vertically aligned on Ti_3C_2 (IE-$MoS_2 \perp Ti_3C_2$) was achieved at four different temperatures (200, 220, 240, and 260 ^oC). For each growth temperature, the electrochemical performance of the IE-$MoS_2 \perp Ti_3C_2$ for HER was determined. The heterostructures obtained at the different growth conditions were characterized with scanning electron microscopy (SEM), scanning tunneling electron microscopy energy dispersive spectroscopy (STEM-EDS), Raman spectroscopy, transmission electron microscopy (TEM), X-ray Photoelectron Spectroscopy (XPS), and X-ray diffraction

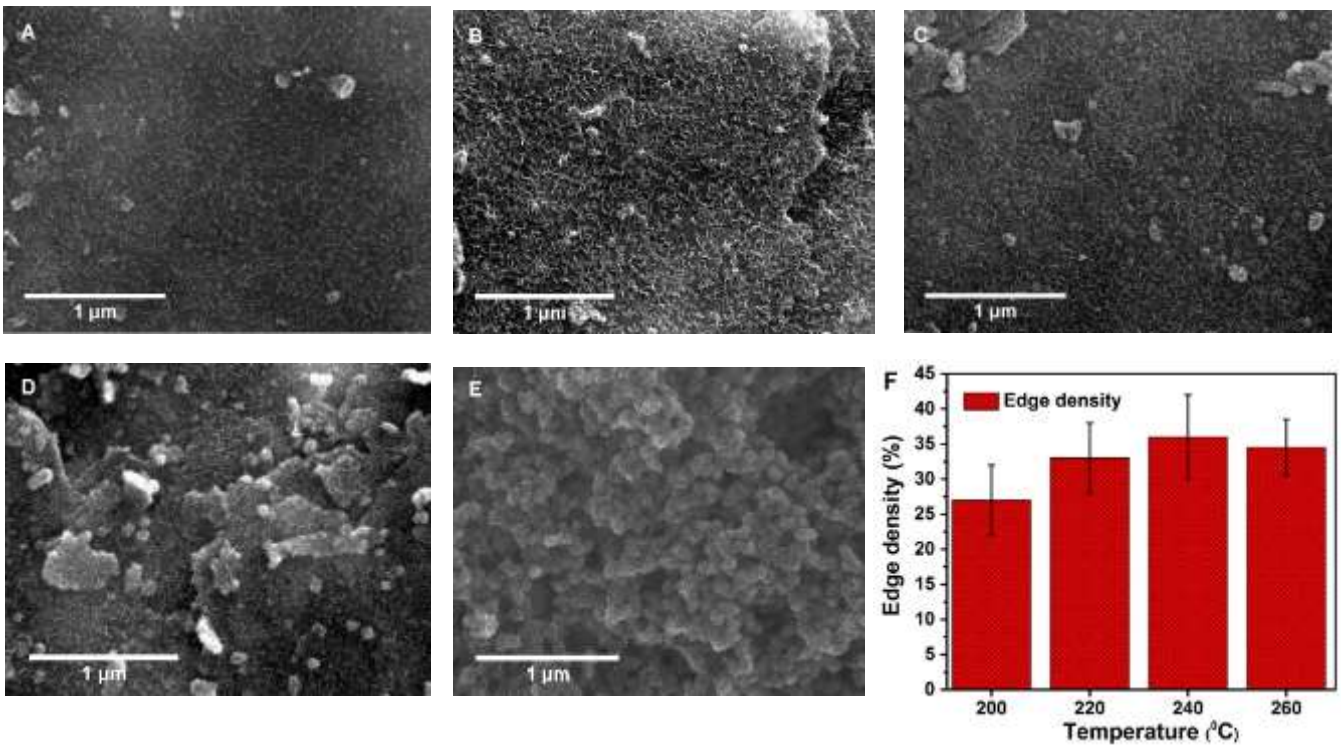

Figure 1: SEM micrographs of IE-$MoS_2 \perp Ti_3C_2$ at growth temperatures of A) 200 ^oC, B) 220 ^oC, C) 240 ^oC, and D) 260 ^oC. E) IE-MoS_2 grown without the MXene substrate. F) Calculated % edge densities of MoS_2 sheets (see supporting information, Figure S1 and Table S1) based on the area of the images as a function of growth temperature. IE-$MoS_2 \perp Ti_3C_2$@240 exhibits the highest edge density without flower-like aggregates (i.e., $MoS_2 \perp Ti_3C_2$@260). Lower growth temperatures (e.g., 200 and 220 ^oC) result in lower MoS_2 edge densities.

(XRD).

SEM micrographs presented in Figure 1 provide direct evidence for the vertically aligned structural motif for IE-$MoS_2 \perp Ti_3C_2$. Analysis of the images (Figure S1 and Table S1) also suggests that the vertically aligned MoS_2 sheets became denser (i.e., area of the edges of MoS_2 relative to the area of the Ti_3C_2 sheets) on the MXene support as the growth temperature was increased from 200 (i.e., IE-$MoS_2 \perp Ti_3C_2$@200) to 240 ^oC (i.e., IE-$MoS_2 \perp Ti_3C_2$@240). IE-$MoS_2 \perp Ti_3C_2$@260 exhibited flower-like aggregates of MoS_2 coexisting with a vertically aligned MoS_2 component (Figure 1D), leading to a reduction in the density of vertically aligned edges of MoS_2 sheets, relative to IE-$MoS_2 \perp Ti_3C_2$@240. We mention that a prior study by Wu *et al.* used a hydrothermal method to obtain vertically aligned MoS_2 on Ti_3C_2 MXene stabilized by carbon nanoplating.[51] In contrast to the microwave synthesis approach, this prior study showed that the Ti_3C_2 MXene support, in the absence of carbon nanoplating, was unstable under hydrothermal synthesis conditions.

Our experimental observations from SEM suggest that at a microwave-assisted synthesis temperature of 260 ^oC there is some formation and nucleation of MoS_2 sheets in solution prior to binding to the MXene support. This homogeneous reaction would appear not to occur at a synthesis temperature of 240 ^oC where formation of MoS_2 sheets during microwave heating occurs exclusively at the MXene surface. At the lower synthesis temperatures (200 and 220 ^oC) we believe that incomplete reduction of the MoS_4^{2-} precursor within the reaction time of 2 h leads to the lower density of vertically aligned MoS_2 sheets. The atomic ratio, Mo:S, of IE-$MoS_2 \perp Ti_3C_2$@240 obtained with EDS was ~1:2 (Figure S2 and S3) consistent with the growth of MoS_2 sheets. A STEM-EDS elemental map of IE-$MoS_2 \perp Ti_3C_2$@240 (Figure S3) shows the distribution of Ti, Mo and

S on the MXene sheets. The SEM images suggest that a growth temperature of 240 ºC is optimal for the synthesis of IE-MoS_2⊥Ti_3C_2, since it led to the highest density of vertically aligned sheets without the presence of flower-like aggregates (Figure 1F).

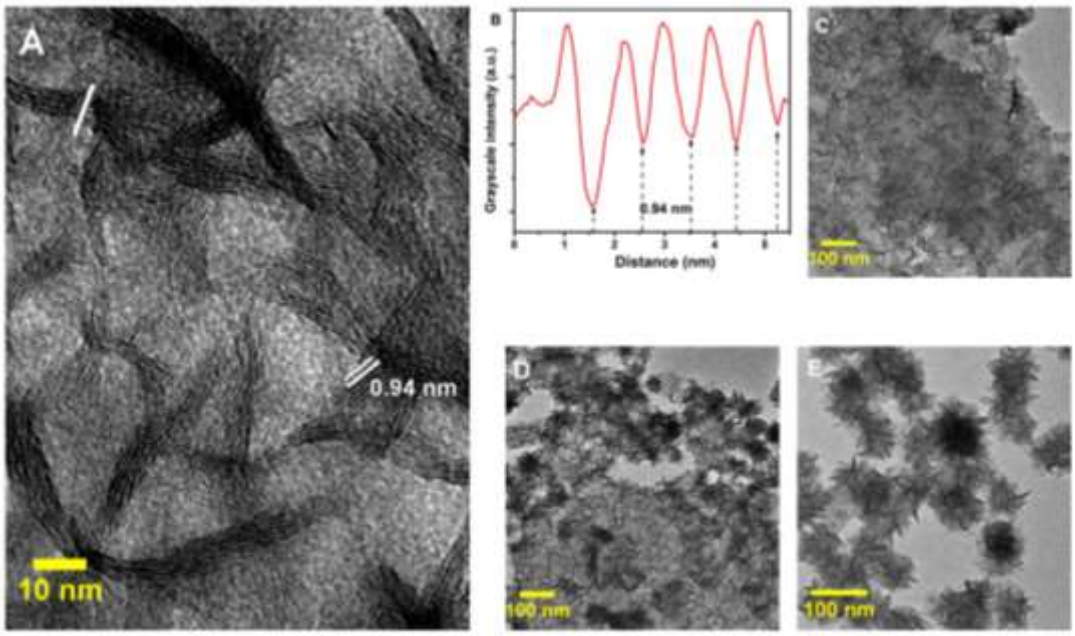

Figure 2: A) HRTEM of IE-MoS_2⊥Ti_3C_2@240 and B) Height profile of MoS_2 along the white line on image 2A, C) and D) TEM images of IE-MoS_2⊥Ti_3C_2@240 and MoS_2⊥Ti_3C_2@260 and E) IE-MoS_2 without the MXene support.

High-resolution TEM (HRTEM) (Figure 2A and Figure S4) was used to characterize the interlayer spacing of IE-MoS_2⊥Ti_3C_2. XRD was not useful for such a determination, since the relatively weak Bragg reflections of the MoS_2 component of IE-MoS_2⊥Ti_3C_2 were obscured by the strong reflections associated with the Ti_3C_2 support (Figure S5). TEM (Figure 2A) shows MoS_2 nano clusters with their edge-on morphology confirming the presence of vertically aligned clusters of sheets in IE-MoS_2⊥Ti_3C_2@240. The number of sheets making up the clusters ranged from two (i.e., a bilayer) to 10 layers. Contrast profiles of these stacked sheets in the HRTEM were used to determine the interlayer

spacing that was associated with IE-$MoS_2 \perp Ti_3C_2$@240 (Figure 2B). Analysis of these data show a uniform interlayer spacing of ~9.4 Å. This spacing does not vary with the synthesis temperature of IE-$MoS_2 \perp Ti_3C_2$ (see Figure S4 for samples synthesized at 200, 220 and 260 ^oC). Previous research showed that the microwave assisted synthesis of unsupported colloidal MoS_2 (using the same precursors as in this study) also gave rise to stacked MoS_2 with an interlayer spacing ~9.4 Å (an expansion of ~3.2 Å relative to 2H-MoS_2).[17-18] To further validate this statement, we synthesized MoS_2 with no MXene (IE-MoS_2@260) and performed XRD on the resulting powder. Analysis of this material showed a similar interlayer spacing of ~9.4 Å (Figure S5). The expansion of the interlayer spacing could be due to the intercalation of oxidized DMF and/or to interlayer NH_4^+ (retained from the $(NH_4)_2MoS_4$ precursor).[17] TEM micrographs in Figure 2 also show that IE-$MoS_2 \perp Ti_3C_2$@240 (Figure 2C) is composed of uniform sheets of MoS_2 vertically aligned on the MXene substrate. With regard to IE-$MoS_2 \perp Ti_3C_2$@260, TEM shows the presence of flower-like aggregates of MoS_2 (Figure 2D) in addition to vertically aligned MoS_2 sheets, consistent with the SEM result shown above. These flower-like structures resemble the aggregates of IE-MoS_2 that grow in the absence of the MXene substrate (Figure 1E and 2E). As mentioned above, this morphology associated with IE-$MoS_2 \perp Ti_3C_2$@260 is likely due to the homogeneous nucleation of $(NH_4)_2MoS_4$ in solution at 260 ^oC in the presence of the microwave electromagnetic field interacting with the ion dipoles of MoS_4^{2-}.[17-18, 48]

Samples were further characterized with Raman spectroscopy. Figure S6 exhibits Raman data for IE-$MoS_2 \perp Ti_3C_2$@240, IE-$MoS_2 \perp Ti_3C_2$@260, and commercially purchased 2H-MoS_2. For the IE-MoS_2 samples, peaks at 402 and 376 cm^{-1} are assigned to

the E^1_{2g} and A_{1g} vibrational modes of MoS_2, respectively. The peaks show a red shift relative to those analogous Raman features associated with 2H-MoS_2 (407 and 381 cm^{-1}) that does not have an expanded interlayer. A possible reason for this shift in vibrational frequencies is that the larger interlayer spacing for IE-$MoS_2 \perp Ti_3C_2$ reduces the coupling between the sheets (relative to reference 2H-MoS_2).[17, 52-53] The intensity of the out-of-plane A_{1g} mode is greater than the in-plane E^1_{2g} mode suggesting that IE-MoS_2 and IE-$MoS_2 \perp Ti_3C_2$ have abundant edge sites with less S-Mo-S interactions in between layers due to the relatively large interlayer spacing.[17] XPS was used to identify the phase and the oxidation states of Mo, S and Ti. Characteristic Mo^{4+} peaks at binding energies of 228.8 and 231.8 eV, corresponding to $3d_{5/2}$ and $3d_{3/2}$ spectroscopic features, respectively, were observed in the fitted spectrum (SI Figure S8A). Moreover, a higher oxidation state Mo species (Mo^{5+}/Mo^{6+}) was apparent. The presence of Mo^{5+}/Mo^{6+} oxidation states have been observed in previous studies and their presence is believed to be due to some oxidation of the $(NH_4)_2MoS_4$ precursor.[32] S 2p XPS shows no oxidation of the S^{2-} groups (Figure S8B). We note that overall, the binding energies of Mo and S are lower in energy (~0.6 eV) than those respective features associated with the semiconducting 2H-MoS_2 phase. This difference could conceivably be due to the differences in electronic structure (i.e., the metallic like 1T-MoS_2 phase versus the semiconductor 2H-MoS_2 phase). Ti-2p XPS shows a range of peaks assigned to various functional groups on the surface (Figure S7 and S8). Ti is primarily bonded to C and O, but spectroscopic features associated with Ti-F are present which presumably results from the etching process, that leads to at least a fraction of the Ti_3C_2 sheets being fluorine terminated.

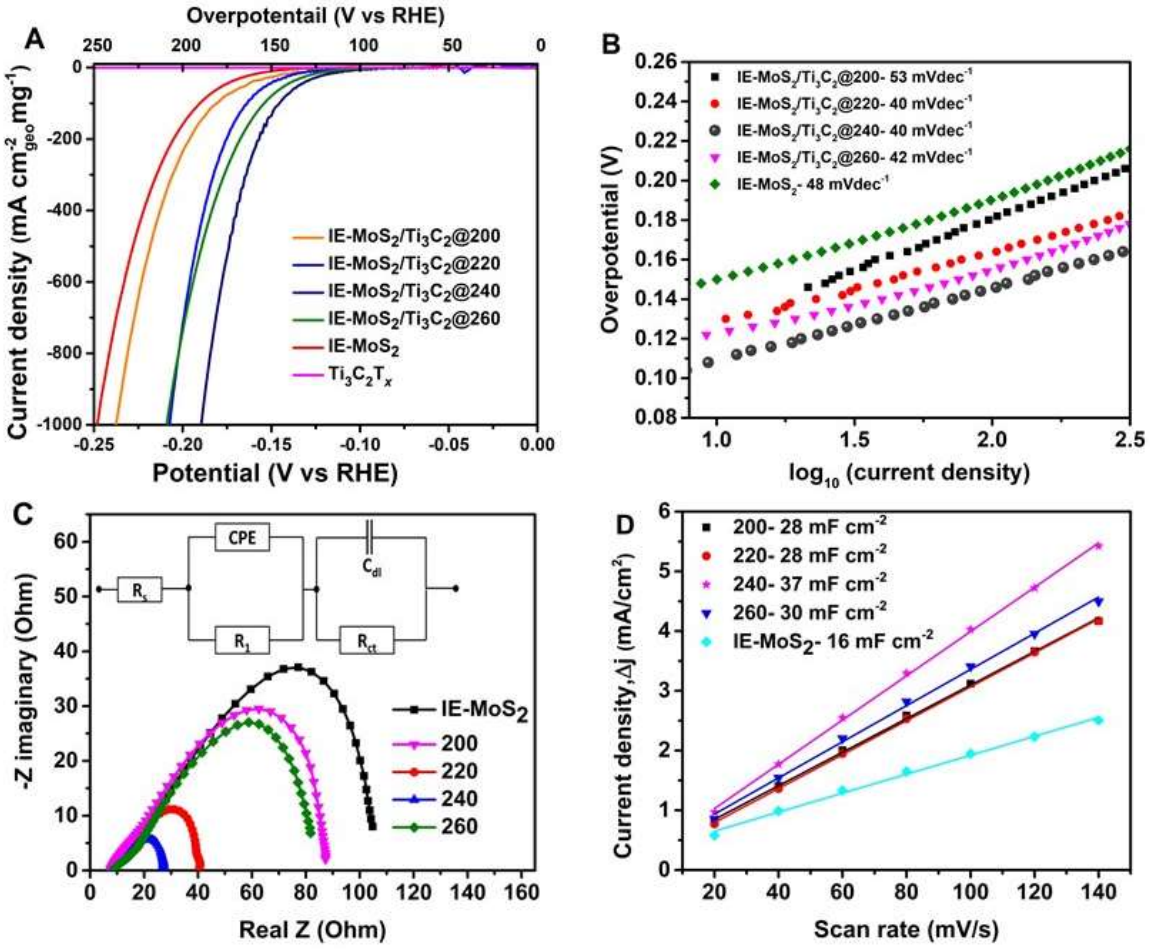

Figure 3: HER kinetics for samples prepared at different temperatures, A) polarization curves of heterostructures synthesized at 200, 220, 240, 260 ^{0}C, and IE-MoS_2 obtained at a scan rate 10 mVs^{-1} in 0.5 M H_2SO_4, B) Tafel plots for the samples derived from the polarization plots of A, C) Impedance spectra (Nyquist plots) inset: equivalent circuit used to stimulate the Nyquist plot where, R_s-solution resistance, CPE-constant phase elements, R_1-resitance in the catalyst, R_{ct}-charge transfer resistance and C_{dl}-double layer capacitance, D) scan rate vs current density (j_0) with C_{dl} values in the legend.

To prepare samples for the determination of catalytic activity for the electrocatalytic HER, MoS_2 with and without MXene support were individually drop-cast on a 3 mm diameter glassy carbon electrode with no added binder. The total mass loading of each sample was 0.071 mg cm^{-2}. As the heterostructure is composed of both MXene and MoS_2,

the samples were decomposed in nitric acid and the concentration of Mo and Ti were determined with Inductive Coupled Plasma Optical Emission Spectrometry (ICP-OES). We used this mass data to normalize the linear sweep voltammetry current densities for MoS_2 and $MoS_2 \perp Ti_3C_2$ samples prepared at different growth temperatures. We believe that normalization based on mass is more revealing, since only the MoS_2 in the heterostructure is active towards HER.[54] Figure 3A (see Figure S9B for polarization plots with a graphite counter electrode) shows the cathodic polarization plots corrected for iR losses in solution. A polarization plot normalized to geometric surface area is included in the SI for comparison (Figure S10). Analysis of the polarization curves shows that the onset (η_0) for the HER for IE-$MoS_2 \perp Ti_3C_2$@240 is ~95 mV (Figure 3A). It is noted that the polarization curves shown were obtained after cycling the catalyst 30 times between 0 and -0.70 V vs RHE (Figure S10B). After cycling, polarization plots with no background capacitive current in the non-faradaic region (i.e, before the onset potential) were obtained. The overpotential (η) to reach a current density of 10 mA/cm^{2}mg for IE-$MoS_2 \perp Ti_3C_2$@240 was 110 mV. At the same current density, IE-MoS_2 deposited on glassy carbon required an overpotential of ~160 mV to achieve a 10 mA/cm^{2}mg current density. We attribute the increased catalytic activity (i.e., lower onset and overpotential) of IE-$MoS_2 \perp Ti_3C_2$@240 for the HER relative to the unsupported MoS_2 to the ease of electron transfer from the substrate to the MoS_2 catalyst. Overall our results show that the current density at 50 mV beyond the onset potential of each sample increases with an increasing density of edge sites (Figure S11). The higher current densities observed for samples synthesized at higher temperatures at a given potential is a result of the availability of more active edge sites. With regard to the Tafel slope, another merit of

electrocatalytic performance, samples synthesized at 220, 240, 260 ^{o}C all had similar values (~40 mV dec^{-1}) to IE-MoS_2 (Figure 3B). The exception was IE-$MoS_2 \perp Ti_3C_2$@200, which had a Tafel slope of 53 mV dec^{-1}. Based on our data, however, we cannot determine why this particular sample had a higher slope. Differences in Tafel slope are typically taken to indicate changes in reaction mechanism. Considering that all our samples contained vertically aligned IE-MoS_2, as the catalytic component, a change in mechanism would not be expected.

Figure 3C exhibits impedance spectra for all the samples investigated in this study. The impedance spectra are not perfect semi circles, implying that there is a charge transfer resistance (R_{ct}) between the electrolyte and the catalyst, as well as a resistance in the catalyst and the substrate (R_1). The charge transfer resistance R_{ct} is lower (6.8 Ω) for $MoS_2 \perp Ti_3C_2$ compared to MoS_2 alone (~48 Ω) for the stimulated circuit shown in the inset of Figure 3C. The higher impedance for IE-$MoS_2 \perp Ti_3C_2$@260 is not surprising given the heterogeneity and agglomeration of MoS_2 sheets into nano flower-like aggregate structures for this sample. The lower charge transfer resistance between the MXene and MoS2 sheets helps improve the catalytic activity of the $MoS_2 \perp Ti_3C_2$ hybrid system. It has been suggested in prior research that the IE motif of MoS_2 allows the MoS_2 sheets to act as monolayer sheets which can allow isotropic electron transfer from substrate to the MoS_2 sheets.[17] This effect is more pronounced in IE-$MoS_2 \perp Ti_3C_2$ which provides a better conductivity for the MoS_2 sheets with the current supplying cathode, reducing R_{ct} for the heterostructures relative to IE-MoS_2 directly deposited on the glassy carbon electrode. The electrochemical double layer capacitance (C_{dl}) value is widely used to determine the electrochemically active surface area (ECSA) of electrocatalysts (Figure

S12), since the value of the C_{dl} is proportional to the ECSA.[55-57] Our data show that all the samples (Figure 3D) have at least twice the active surface area compared to IE-MoS_2. The improved activity for IE-$MoS_2 \perp Ti_3C_2$@240 is also reflected by it having the highest ECSA value among all the samples in this study. Chronopotentiometry was used to evaluate the stability of the electrocatalysts during the HER. Figure S13 shows the chronopotentiometric curve for IE-$MoS_2 \perp Ti_3C_2$@240 and IE-MoS_2 for a reaction time of 20 h, carried out at a current density of 10 mA cm^{-2}_{geo}. Both samples show excellent catalyst stability, with each sample showing less than a 7% change in the potential required to maintain 10 mA cm^{-2} during the 20 h period. Polarization plots obtained after the stability test (Figure S14) showed little difference from the respective polarization plots obtained before the test.

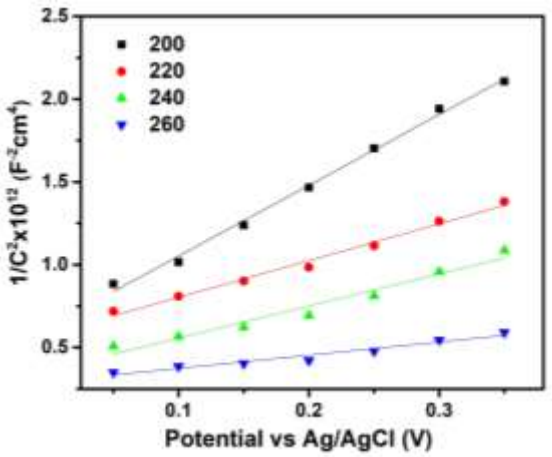

Figure 4: Mott Schottky plots for $MoS_2 \perp Ti_3C_2$ heterostructures prepared at different temperatures of 200, 220, 240 and 260 ^oC obtained in 0.5 M Na_2SO_4.

The presence of a Schottky-like barrier (metal-semiconductor junction) between the metallic Ti_3C_2 and semiconducting MoS_2 can have an effect on the onset potential for the $MoS_2 \perp Ti_3C_2$ samples. We believe the difference in the onset potential for samples at different temperatures to be a result of the energy barrier for charge transfer between the MXene and MoS_2 interface. The carrier concentration of the different $MoS_2 \perp Ti_3C_2$ samples were investigated using the linear region of the Mott Schottky plots. The inverse value of the slope of these plots is proportional to the carrier density of the catalyst.[58-60] Analysis of the data shows that there is a direct correlation between the charge carrier concentration and the activity of the samples. The positive slopes of the Mott Schottky plots in Figure 4 are characteristic of n-type semiconductors.[58, 60-61] The formation of a Schottky barrier can result in an energetic penalty for electron transfer. The lower the barrier, the faster the electron transfer between the interface and catalyst. With a higher carrier concentration in MoS_2 this barrier would be more like a metal-metal junction with no barrier, thus causing enhanced electron transfer.[60] For samples synthesized at higher temperatures (240 and 260 ^oC) the carrier density is significantly higher than the samples synthesized at lower temperatures (200 and 220 ^oC). The carrier concentrations are summarized in Table S2.

Table 1: Comparison of onset potentials and Tafel slopes of studies on vertically aligned MoS_2 synthesized on different substrates.

Catalysts	Synthesis technique	Onset potential (mV vs RHE)[d]	Tafel slope (mV/dec)	Ref.
[a]VA-MoS_2 on Glassy carbon	Thermal evaporation	-250	105-120	Kong *et al.*[20]
[b]VO-MoS_2 on carbon cloth	Solvothermal	-100	50	Yan *et al.*[29]
MoS_2 nanoparticles on graphene	Solvothermal	-100	41	Li *et al.*[31]
IE-MoS_2 on [c]GO/rGO	Microwave	-75	63	Chatti *et al.*[32]
Self-templated 1T-2H MoS_2	Solvothermal	-119	60	Xiang *et al.*[33]
1T-MoS_2 on glassy carbon	Thermal evaporation	-110	44	Wang *et al.*[34]
VA-MoS_2 on carbon cloth	Hydrothermal	-100	39	Zhang *et al.*[28]
IE-MoS_2 on rGO	Microwave	-117	42	Sun *et al.*[18]
MoS_2 on Ti_3C_2 with carbon nanoplating	Hydrothermal	-20	45	Wu *et al.*[51]
IE-MoS_2 on Ti_3C_2 MXene	Microwave	-95	40	This work

([a] VA-vertically aligned, [b] VO- vertically oriented, [c] GO-graphene oxide). [d] Onset potentials were derived from their respective Tafel plots.

Conclusions

Table 1 summarizes the results from relevant literature for vertically aligned MoS_2 on a range of substrates. A comparison of the HER onset for IE-MoS_2⊥Ti_3C_2@240 to those obtained in prior studies for other vertically aligned samples shows that IE-MoS_2⊥Ti_3C_2@240 is one of the most active materials to date. It is noted that while IE-MoS_2⊥Ti_3C_2@240 exhibits a relatively low overpotential for the HER, the value is comparable to vertically aligned MoS_2 on reduced graphene oxide.[32] We mention that

MoS_2 grown on carbon nanoplated Ti_3C_2[51] exhibits a low onset potential of -20 mV, but it is noted that in the same study the hydrothermal synthesis of MoS_2 on MXene without nanoplating led to oxidation of Ti_3C_2 and a relatively high onset potential of -260 mV. Based in part on this comparison, we contend that the microwave synthetic method for IE-MoS_2⊥Ti_3C_2 detailed in this contribution is a scalable and relatively fast synthetic method using Earth abundant materials to produce a highly active MoS_2 catalyst for the HER. The improved activity is attributed to the enhanced conductivity between the highly conductive MXene and IE-MoS_2 and also the higher carrier densities in the MoS_2 and higher number of exposed edges of the catalyst. This high activity taken together with the excellent stability of the IE-MoS_2⊥Ti_3C_2 catalyst makes the material a potentially attractive electrocatalyst for HER in the context of clean energy generation.

Conflicts of interest

"There are no conflicts to declare".

Funding Sources

This work was supported by the Center for the Computational Design of Functional Layered Materials, an Energy Frontier Research Center funded by the U.S. Department of Energy, Office of Science, Basic Energy Sciences under Award # DE-SC0012575.

Notes and references

1. Dresselhaus, M. S.; Thomas, I. L., Alternative energy technologies. *Nature* **2001,** *414,* 332-337.
2. Turner, J. A., Sustainable Hydrogen Production. *Science* **2004,** *305*, 972-974.

3. Lewis, N. S.; Nocera, D. G., Powering the planet: Chemical challenges in solar energy utilization. *Proc. Nat. Acad. Sci.* **2006,** *103*, 15729-15735.
4. Bockris, J. O. M., The hydrogen economy: Its history. *International Journal of Hydrogen Energy* **2013,** *38*, 2579-2588.
5. Walter, M. G.; Warren, E. L.; McKone, J. R.; Boettcher, S. W.; Mi, Q.; Santori, E. A.; Lewis, N. S., Solar Water Splitting Cells. *Chem. Rev.* **2010,** *110*, 6446-6473.
6. Jaramillo, T. F.; Jørgensen, K. P.; Bonde, J.; Nielsen, J. H.; Horch, S.; Chorkendorff, I., Identification of Active Edge Sites for Electrochemical H_2 Evolution from MoS_2 Nanocatalysts. *Science* **2007,** *317*, 100-102.
7. Nørskov, J. K.; Bligaard, T.; Logadottir, A.; Kitchin, J. R.; Chen, J. G.; Pandelov, S.; Stimming, U., Trends in the Exchange Current for Hydrogen Evolution. *J. Electrochem. Soc.* **2005,** *152*, J23-J26.
8. Greeley, J.; Jaramillo, T. F.; Bonde, J.; Chorkendorff, I.; Norskov, J. K., Computational high-throughput screening of electrocatalytic materials for hydrogen evolution. *Nat Mater* **2006,** *5*, 909-913.
9. Hinnemann, B.; Moses, P. G.; Bonde, J.; Jørgensen, K. P.; Nielsen, J. H.; Horch, S.; Chorkendorff, I.; Nørskov, J. K., Biomimetic Hydrogen Evolution: MoS_2 Nanoparticles as Catalyst for Hydrogen Evolution. *J. Am. Chem. Soc.* **2005,** *127*, 5308-5309.
10. Benck, J. D.; Hellstern, T. R.; Kibsgaard, J.; Chakthranont, P.; Jaramillo, T. F., Catalyzing the Hydrogen Evolution Reaction (HER) with Molybdenum Sulfide Nanomaterials. *ACS Catal.* **2014,** *4*, 3957-3971.
11. Chhowalla, M.; Shin, H. S.; Eda, G.; Li, L.-J.; Loh, K. P.; Zhang, H., The chemistry of two-dimensional layered transition metal dichalcogenide nanosheets. *Nat. Chem.* **2013,** *5*, 263-275.
12. Guo, Y.; Tang, J.; Qian, H.; Wang, Z.; Yamauchi, Y., One-Pot Synthesis of Zeolitic Imidazolate Framework 67-Derived Hollow Co_3S_4@MoS_2 Heterostructures as Efficient Bifunctional Catalysts. *Chemistry of Materials* **2017,** *29*, 5566-5573.
13. Li, G.; Zhang, D.; Qiao, Q.; Yu, Y.; Peterson, D.; Zafar, A.; Kumar, R.; Curtarolo, S.; Hunte, F.; Shannon, S., et al., All The Catalytic Active Sites of MoS_2 for Hydrogen Evolution. *J. Am. Chem. Soc.* **2016,** *138*, 16632-16638.
14. Attanayake, N. H.; Thenuwara, A. C.; Patra, A.; Aulin, Y. V.; Tran, T. M.; Chakraborty, H.; Borguet, E.; Klein, M. L.; Perdew, J. P.; Strongin, D. R., Effect of Intercalated Metals on the Electrocatalytic Activity of 1T-MoS2 for the Hydrogen Evolution Reaction. *ACS Energy Lett.* **2018,** *3*, 7-13.
15. Chua, C. K.; Loo, A. H.; Pumera, M., Top-Down and Bottom-Up Approaches in Engineering 1 T Phase Molybdenum Disulfide (MoS_2): Towards Highly Catalytically Active Materials. *Chem. Eur. J* **2016,** *22*, 14336-14341.
16. Kibsgaard, J.; Chen, Z.; Reinecke, B. N.; Jaramillo, T. F., Engineering the surface structure of MoS_2 to preferentially expose active edge sites for electrocatalysis. *Nat Mater* **2012,** *11*, 963-969.
17. Gao, M.-R.; Chan, M. K. Y.; Sun, Y., Edge-terminated molybdenum disulfide with a 9.4-Å interlayer spacing for electrochemical hydrogen production. *Nat. Commun.* **2015,** *6*, 7493.
18. Sun, Y.; Alimohammadi, F.; Zhang, D.; Guo, G., Enabling Colloidal Synthesis of Edge-Oriented MoS_2 with Expanded Interlayer Spacing for Enhanced HER Catalysis. *Nano Lett.* **2017,** *17*, 1963-1969.

19. Chia, X.; Eng, A. Y. S.; Ambrosi, A.; Tan, S. M.; Pumera, M., Electrochemistry of Nanostructured Layered Transition-Metal Dichalcogenides. *Chem. Rev.* **2015,** *115*, 11941-11966.
20. Kong, D.; Wang, H.; Cha, J. J.; Pasta, M.; Koski, K. J.; Yao, J.; Cui, Y., Synthesis of MoS2 and MoSe2 Films with Vertically Aligned Layers. *Nano Lett.* **2013,** *13*, 1341-1347.
21. Rasamani, K. D.; Alimohammadi, F.; Sun, Y., Interlayer-expanded MoS_2. *Mater. Today* **2017,** *20*, 83-91.
22. Qinbai, Y.; Qipeng, L.; Xiao, Z.; Chaoliang, T.; Hua, Z., Three-Dimensional Architectures Constructed from Transition-Metal Dichalcogenide Nanomaterials for Electrochemical Energy Storage and Conversion. *Angew. Chem. Int. Ed.* **2018,** *57*, 626-646.
23. Zou, X.; Zhang, Y., Noble metal-free hydrogen evolution catalysts for water splitting. *Chemical Society Reviews* **2015,** *44*, 5148-5180.
24. B., Z. M.; Cuiling, L.; Qingmin, J.; Bo, J.; Satoshi, T.; Yusuke, I.; P., H. J.; Katsuhiko, A.; Yusuke, Y., Self-Construction from 2D to 3D: One-Pot Layer-by-Layer Assembly of Graphene Oxide Sheets Held Together by Coordination Polymers. *Angew. Chem. Int. Ed.* **2016,** *55*, 8426-8430.
25. Zheng, B.; Chen, Y.; Qi, F.; Wang, X.; Zhang, W.; Li, Y.; Li, X., 3D-hierarchical $MoSe_2$ nanoarchitecture as a highly efficient electrocatalyst for hydrogen evolution. *2D Mater.* **2017,** *4*, 025092.
26. Yuan, H.; Li, J.; Yuan, C.; He, Z., Facile Synthesis of MoS_2@CNT as an Effective Catalyst for Hydrogen Production in Microbial Electrolysis Cells. *ChemElectroChem* **2014,** *1*, 1828-1833.
27. Zhou, K.; Liu, J.; Shi, Y.; Jiang, S.; Wang, D.; Hu, Y.; Gui, Z., MoS2 Nanolayers Grown on Carbon Nanotubes: An Advanced Reinforcement for Epoxy Composites. *ACS App. Mater. Interfaces* **2015,** *7*, 6070-6081.
28. Zhang, N.; Gan, S.; Wu, T.; Ma, W.; Han, D.; Niu, L., Growth Control of MoS_2 Nanosheets on Carbon Cloth for Maximum Active Edges Exposed: An Excellent Hydrogen Evolution 3D Cathode. *ACS App. Mater. Interfaces* **2015,** *7*, 12193-12202.
29. Yan, Y.; Xia, B.; Li, N.; Xu, Z.; Fisher, A.; Wang, X., Vertically oriented MoS_2 and WS_2 nanosheets directly grown on carbon cloth as efficient and stable 3-dimensional hydrogen-evolving cathodes. *J. Mater. Chem. A* **2015,** *3*, 131-135.
30. Liu, A.; Zhao, L.; Zhang, J.; Lin, L.; Wu, H., Solvent-Assisted Oxygen Incorporation of Vertically Aligned MoS_2 Ultrathin Nanosheets Decorated on Reduced Graphene Oxide for Improved Electrocatalytic Hydrogen Evolution. *ACS App. Mater. Interfaces* **2016,** *8*, 25210-25218.
31. Li, Y.; Wang, H.; Xie, L.; Liang, Y.; Hong, G.; Dai, H., MoS2 Nanoparticles Grown on Graphene: An Advanced Catalyst for the Hydrogen Evolution Reaction. *J. Am. Chem. Soc.* **2011,** *133*, 7296-7299.
32. Chatti, M.; Gengenbach, T.; King, R.; Spiccia, L.; Simonov, A. N., Vertically Aligned Interlayer Expanded MoS_2 Nanosheets on a Carbon Support for Hydrogen Evolution Electrocatalysis. *Chem. of Mater.* **2017,** *29*, 3092-3099.
33. Xiang, T.; Fang, Q.; Xie, H.; Wu, C.; Wang, C.; Zhou, Y.; Liu, D.; Chen, S.; Khalil, A.; Tao, S., et al., Vertical 1T-MoS_2 nanosheets with expanded interlayer spacing edged on a graphene frame for high rate lithium-ion batteries. *Nanoscale* **2017,** *9*, 6975-6983.
34. Wang, H.; Lu, Z.; Xu, S.; Kong, D.; Cha, J. J.; Zheng, G.; Hsu, P.-C.; Yan, K.; Bradshaw, D.; Prinz, F. B., et al., Electrochemical tuning of vertically aligned MoS_2 nanofilms and its

application in improving hydrogen evolution reaction. *Proc. Nat. Acad. Sci.* **2013,** *110*, 19701-19706.
35. Naguib, M.; Mochalin, V. N.; Barsoum, M. W.; Gogotsi, Y., 25th Anniversary Article: MXenes: A New Family of Two-Dimensional Materials. *Adv. Mater.* **2014,** *26*, 992-1005.
36. Naguib, M.; Mashtalir, O.; Carle, J.; Presser, V.; Lu, J.; Hultman, L.; Gogotsi, Y.; Barsoum, M. W., Two-Dimensional Transition Metal Carbides. *ACS Nano* **2012,** *6*, 1322-1331.
37. Anasori, B.; Lukatskaya, M. R.; Gogotsi, Y., 2D metal carbides and nitrides (MXenes) for energy storage. *Nat Rev Mater.* **2017,** *2*, 16098.
38. Dillon, A. D.; Ghidiu, M. J.; Krick, A. L.; Griggs, J.; May, S. J.; Gogotsi, Y.; Barsoum, M. W.; Fafarman, A. T., Highly Conductive Optical Quality Solution-Processed Films of 2D Titanium Carbide. *Adv. Funct. Mater.* **2016,** *26*, 4162-4168.
39. Halim, J.; Kota, S.; Lukatskaya, M. R.; Naguib, M.; Zhao, M.-Q.; Moon, E. J.; Pitock, J.; Nanda, J.; May, S. J.; Gogotsi, Y., et al., Synthesis and Characterization of 2D Molybdenum Carbide (MXene). *Adv. Func. Mater.* **2016,** *26*, 3118-3127.
40. Zhang, C.; Anasori, B.; Seral-Ascaso, A.; Park, S.-H.; McEvoy, N.; Shmeliov, A.; Duesberg, G. S.; Coleman, J. N.; Gogotsi, Y.; Nicolosi, V., Transparent, Flexible, and Conductive 2D Titanium Carbide (MXene) Films with High Volumetric Capacitance. *Adv. Mater.* **2017,** *29*, 1702678-n/a.
41. Pandey, M.; Thygesen, K. S., Two-Dimensional MXenes as Catalysts for Electrochemical Hydrogen Evolution: A Computational Screening Study. *J. Phys. Chem. C* **2017,** *121*, 13593-13598.
42. Handoko, A. D.; Fredrickson, K. D.; Anasori, B.; Convey, K. W.; Johnson, L. R.; Gogotsi, Y.; Vojvodic, A.; Seh, Z. W., Tuning the Basal Plane Functionalization of Two-Dimensional Metal Carbides (MXenes) To Control Hydrogen Evolution Activity. *ACS Appl. Energy Mater.* **2018,** *1*, 173-180.
43. Romer, F. M.; Wiedwald, U.; Strusch, T.; Halim, J.; Mayerberger, E.; Barsoum, M. W.; Farle, M., Controlling the conductivity of Ti_3C_2 MXenes by inductively coupled oxygen and hydrogen plasma treatment and humidity. *RSC Adv.* **2017,** *7*, 13097-13103.
44. Halim, J.; Lukatskaya, M. R.; Cook, K. M.; Lu, J.; Smith, C. R.; Näslund, L.-Å.; May, S. J.; Hultman, L.; Gogotsi, Y.; Eklund, P., et al., Transparent Conductive Two-Dimensional Titanium Carbide Epitaxial Thin Films. *Chem. Mater.* **2014,** *26*, 2374-2381.
45. Xiang, T.; Fang, Q.; Xie, H.; Wu, C.; Wang, C.; Zhou, Y.; Liu, D.; Chen, S.; Khalil, A.; Tao, S., et al., Vertical 1T-MoS_2 nanosheets with expanded interlayer spacing edged on a graphene frame for high rate lithium-ion batteries. *Nanoscale* **2017**.
46. Horikoshi, S.; Osawa, A.; Abe, M.; Serpone, N., On the Generation of Hot-Spots by Microwave Electric and Magnetic Fields and Their Impact on a Microwave-Assisted Heterogeneous Reaction in the Presence of Metallic Pd Nanoparticles on an Activated Carbon Support. *J. Phys. Chem. C* **2011,** *115*, 23030-23035.
47. Zhu, Y.-J.; Chen, F., Microwave-Assisted Preparation of Inorganic Nanostructures in Liquid Phase. *Chem. Rev.* **2014,** *114*, 6462-6555.
48. Gawande, M. B.; Shelke, S. N.; Zboril, R.; Varma, R. S., Microwave-Assisted Chemistry: Synthetic Applications for Rapid Assembly of Nanomaterials and Organics. *Acc. Chem. Res.* **2014,** *47*, 1338-1348.
49. Shahzad, F.; Alhabeb, M.; Hatter, C. B.; Anasori, B.; Man Hong, S.; Koo, C. M.; Gogotsi, Y., Electromagnetic interference shielding with 2D transition metal carbides (MXenes). *Science* **2016,** *353*, 1137-1140.

50. Qing, Y.; Zhou, W.; Luo, F.; Zhu, D., Titanium carbide (MXene) nanosheets as promising microwave absorbers. *Ceram. Int.* **2016,** *42*, 16412-16416.
51. Wu, X.; Zhiyu, W.; Mengzhou, Y.; Luyang, X.; Jieshan, Q., Stabilizing the MXenes by Carbon Nanoplating for Developing Hierarchical Nanohybrids with Efficient Lithium Storage and Hydrogen Evolution Capability. *Adv. Mat.* **2017,** *29*, 1607017.
52. Liu, K.; Zhang, L.; Cao, T.; Jin, C.; Qiu, D.; Zhou, Q.; Zettl, A.; Yang, P.; Louie, S. G.; Wang, F., Evolution of interlayer coupling in twisted molybdenum disulfide bilayers. *Nat. Commun.* **2014,** *5*, 4966.
53. Lee, C.; Yan, H.; Brus, L. E.; Heinz, T. F.; Hone, J.; Ryu, S., Anomalous Lattice Vibrations of Single- and Few-Layer MoS_2. *ACS Nano* **2010,** *4*, 2695-2700.
54. Handoko, A. D.; Fredrickson, K. D.; Anasori, B.; Convey, K. W.; Johnson, L. R.; Gogotsi, Y.; Vojvodic, A.; Seh, Z. W., Tuning the Basal Plane Functionalization of Two-Dimensional Metal Carbides (MXenes) To Control Hydrogen Evolution Activity. *ACS Applied Energy Materials* **2018,** *1*, 173-180.
55. Thenuwara, A. C.; Shumlas, S. L.; Attanayake, N. H.; Aulin, Y. V.; McKendry, I. G.; Qiao, Q.; Zhu, Y.; Borguet, E.; Zdilla, M. J.; Strongin, D. R., Intercalation of Cobalt into the Interlayer of Birnessite Improves Oxygen Evolution Catalysis. *ACS Catal.* **2016,** *6*, 7739-7743.
56. Thenuwara, A. C.; Attanayake, N. H.; Yu, J.; Perdew, J. P.; Elzinga, E. J.; Yan, Q.; Strongin, D. R., Cobalt Intercalated Layered NiFe Double Hydroxides for the Oxygen Evolution Reaction. *The Journal of Physical Chemistry B* **2018,** *122*, 847-854.
57. Li, C.; Jiang, B.; Miyamoto, N.; Kim, J. H.; Malgras, V.; Yamauchi, Y., Surfactant-Directed Synthesis of Mesoporous Pd Films with Perpendicular Mesochannels as Efficient Electrocatalysts. *J. Am. Chem. Soc.* **2015,** *137*, 11558-11561.
58. Zhang, L.; Sun, L.; Huang, Y.; Sun, Y.; Hu, T.; Xu, K.; Ma, F., Hydrothermal synthesis of N-doped RGO/$MoSe_2$ composites and enhanced electro-catalytic hydrogen evolution. *J. Mater. Sci.* **2017,** *52*, 13561-13571.
59. Kirchartz, T.; Gong, W.; Hawks, S. A.; Agostinelli, T.; MacKenzie, R. C. I.; Yang, Y.; Nelson, J., Sensitivity of the Mott–Schottky Analysis in Organic Solar Cells. *J. Phys. Chem. C* **2012,** *116*, 7672-7680.
60. Basirun, W. J.; Sookhakian, M.; Baradaran, S.; Endut, Z.; Mahmoudian, M. R.; Ebadi, M.; Yousefi, R.; Ghadimi, H.; Ahmed, S., Graphene oxide electrocatalyst on MnO_2 air cathode as an efficient electron pump for enhanced oxygen reduction in alkaline solution. *Sci. Rep.* **2015,** *5*, 9108.
61. Cong, Y.; Park, H. S.; Wang, S.; Dang, H. X.; Fan, F.-R. F.; Mullins, C. B.; Bard, A. J., Synthesis of Ta_3N_5 Nanotube Arrays Modified with Electrocatalysts for Photoelectrochemical Water Oxidation. *J. Phys. Chem. C* **2012,** *116*, 14541-14550.

BRIEFS. Vertically aligned interlayer expanded (IE) MoS_2 on $Ti_3C_2T_x$ (MXene) support as an efficient electrocatalytic HER catalyst.

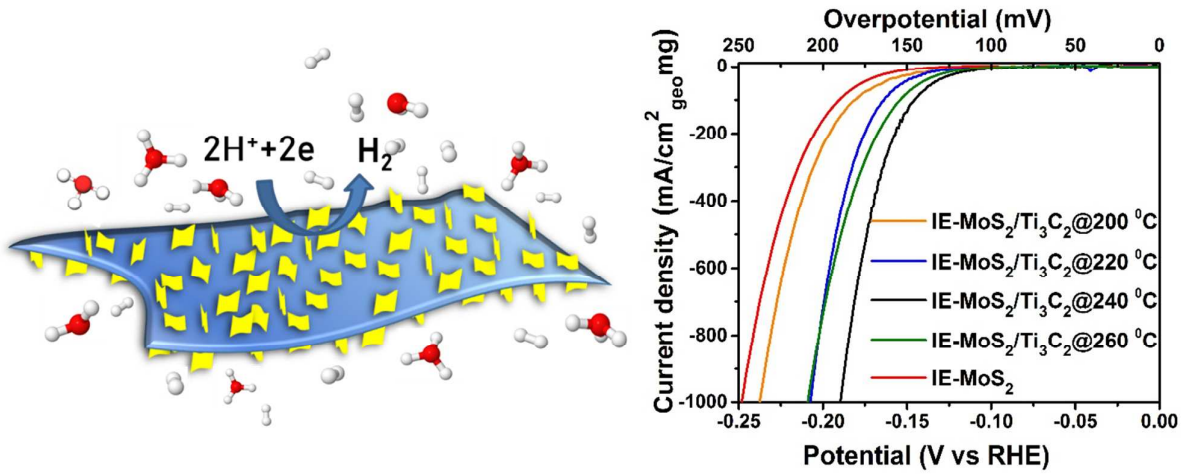

TOC figure